OPTICAL FIBER BENDING SENSOR BASED ON SPECKLE PATTERN IMAGING

Isa NAVRUZ[1], Ceren DILSIZ[1], Eylul Sevim ORTAK[1], Sevde Nur BOYRAZ[1]

[1] Department of Electrical and Electronics Engineering, Ankara University, Ankara, TÜRKİYE

ABSTRACT. In this paper, we propose a new fiber bending sensor based on speckle pattern imaging. The design and implementation of the sensor are demonstrated by simulated studies. The speckle pattern imaging technique by using a multimode fiber can offer high spatial resolution. In this study, we showed that the bending sensor responds very sensitively by using the correlation of the images. The fiber sensing part consists of a curve in a form similar to the S structure. We reached a sensitivity of 0.0295 μm^{-1} by bending the fiber only 60°. Sensitivity can be further increased by reducing the bending diameter or creating a full loop.

1. INTRODUCTION

Fiber optic sensors have emerged as a powerful and versatile technology for measuring various physical parameters with high accuracy and sensitivity. They use the basic principles of light transmission and modulation within optical fibers to measure. Unlike conventional sensors that rely on electrical or mechanical components, fiber optic sensors exploit the interaction between light and the surrounding environment to detect and quantify changes in temperature [1,2 3, 4], strain [5, 6, 7], pressure [8, 9, 10], humidity [11, 12, 13, 14], chemical composition [15, 16, 17, 18] and more. This ability to convert physical quantities into measurable optical signals has opened up new avenues for highly sensitive and reliable sensing. Fiber optic sensors offer numerous advantages such as small size, immunity to electromagnetic interference, remote sensing capability, and the ability to multiplex

multiple sensors along a single fiber. These advantages have prompted extensive research into the development of novel fiber optic sensing techniques, including those based on the analysis of speckle patterns.

In recent years, there has been a growing interest in the development of optical fiber bending sensors due to their numerous applications in various fields, including structural health monitoring, robotics, biomechanics, and industrial automation. These sensors utilize the unique properties of optical fibers to detect and measure bending-induced deformations, providing accurate and reliable information about the bending curvature and applied forces. Researchers have used different techniques to measure bending, based on modulation principles such as intensity, wavelength, and frequency modulation [19, 20, 21, 22]. In addition, they have proposed fiber bending devices using different types of fibers such as single mode fiber, multimode fiber, multicore fiber, fiber Bragg grating or long period fiber grating. In a significant part of these studies, bending measurement is performed by calculating the intensity or optical power loss at a standard single or multi-mode fiber output [23, 24]. In others, measurement is performed by analyzing changes in the wavelength spectrum resulting from modal interference. Although bending sensors based on wavelength or frequency modulation are more sensitive to curvature than those based on intensity modulation, the optical spectrum analyzer used in such systems causes a high cost and compromises the compact structure of the sensor.

In this paper, we propose a new fiber bending sensor based on speckle pattern imaging. The use of speckle pattern imaging as a detection mechanism in fiber optic bending sensors offers many advantages. First, it enables non-contact sensing and the quantity to be measured with the sensor eliminates the need for physical contact. Secondly, the speckle pattern imaging technique offers high spatial resolution. Moreover, it will be sufficient to use only one camera instead of using an expensive optical spectrum analyzer.

We organized the paper in four chapter. In the second chapter, the propagation of modes in optical fibers and the formation of the speckle pattern image are presented with a theoretical perspective. In the third chapter, the design and implementation of the optical fiber bending sensor based on speckle pattern imaging is demonstrated by simulated studies. The simulation results and bending sensitivity of the sensor are discussed in the fourth section.

2. The formation of speckle pattern image in optical fibers

Optical fibers used in the modern communication industry are the most critical passive optical components that carry the signal in the communication infrastructure. Single-mode fibers are generally preferred for applications that require high data rates or long distances. They are used for very long-distance connections such as

telecommunications, cable TV, applications requiring long-distance data transmission, and even transatlantic undersea link. On the other hand, multimode fibers are often used in many applications such as short-distance local area networks, decorative lighting as a light source, and transporting light from a high-power optical source to the place where it is needed. Fig. 1 (a) and (b) show the distribution of light in the cross-sectional area of single mode and multimode fiber, respectively. As seen in the figure, while in a single-mode fiber the light creates a spot appearance similar to a Gaussian distribution, in a multimode fiber this appearance turns into a complex pattern consisting of many small spots. In fact, this is a result of this fiber carrying multiple light rays or modes simultaneously.
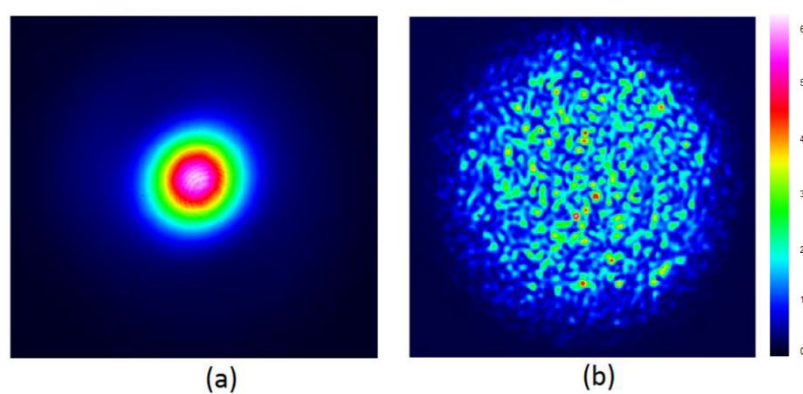

FIGURE 1. Intensity distribution of light at the end of the fiber, (a) Single mode fiber (b) Multimode fiber.

Optical fibers have a radial symmetry. In a multimode step index fiber, hundreds or even thousands of optical modes can be propagated. Since the index profiles exhibit only a small index contrast, they can be assumed to be weakly guiding. In this case, the calculation of fiber modes can be greatly simplified and we can calculate linearly polarized LP modes. The general wave equation in cylindrical coordinates can be written as follows [25].

$$\frac{\partial^2 E}{\partial r^2} + \frac{1}{r}\frac{\partial E}{\partial r} + \frac{1}{r^2}\frac{\partial^2 E}{\partial \varphi^2} + (k^2 - \beta^2)E = 0 \tag{1}$$

Here $E(r, \varphi)$ is the complex electric field, $k = 2\pi/\lambda$ is the wave number, β is the phase constant (imaginary part of the propagation constant) and λ is the vacuum wavelength. If a laser beam with an intensity distribution similar to Gaussian is

applied to the input of a multimode fiber (z=0), the explanation of the complex electric field is as follows:

$$E_{in}(r, \phi) = \frac{1}{\rho} exp \left[-\frac{r^2}{\rho^2} \right] exp(-ik\theta r cos\phi) \tag{2}$$

Here ρ is the Gaussian beam radius at the waist and θ is the angle of the incident Gaussian beam relative to the optical fiber axis. Any guided field distribution in the multimode fiber can be considered as a superposition of all guided modes. So that the light field traveling along the fiber can be written as the sum of the lights coupled to linear polarization modes:

$$E_{in}(r, \phi) = \sum_m \sum_n \alpha_{mn} LP_{mn}(r, \phi) \tag{3}$$

Here α_{mn} is the mode field amplitude, LP_{mn} is any linearly polarized mode and the pair m-n represent to indices of the LP_{mn} mode. Any LP_{mn} filed is calculated with two separate functions, inside and outside the area surrounded by the fiber core radius. At the entrance of the fiber corresponding to the z=0 position, these fields can be calculated with the following equations using Bessel functions

$$LP_{mn}(r, \phi) = \begin{cases} A \frac{1}{J_m(U)} J_m \left(\frac{U_r}{a} \right) cos(m\varphi) & r \leq a \\ A \frac{1}{K_m(W)} K_m \left(\frac{W_r}{a} \right) cos(m\varphi) & r \geq a \end{cases} \tag{4}$$

Here A is a constant, a is the core radius, J_m and K_m are the Bessel and modified Bessel functions, U and W are normalized transfer propagation constants for $r \leq a$ and $r \geq a$, respectively. The relationships among U, W and normalized frequency V are defined by the equations given below.

$$U = a(k^2 n_1^2 - \beta^2)^{\frac{1}{2}}$$
$$W = a(\beta^2 - k^2 n_2^2)^{\frac{1}{2}} \tag{5}$$
$$V^2 = U^2 + W^2 = a^2 k^2(n_1^2 - n_2^2)$$

By solving the above equations numerically, we can obtain the intensity or power distribution of each mode. The speckle patterns in optical fibers result from the interference of optical modes that have traveled different paths within the fiber, leading to a random pattern of bright and dark spots as seen in Fig. 1(b). By summing

all the modes guided by the multimode fiber, we can easily calculate numerically the speckle pattern at the incident end of the fiber. The figure 2 shows the patterns of several lower order modes, including the fundamental mode, and the speckle pattern formed by these modes.
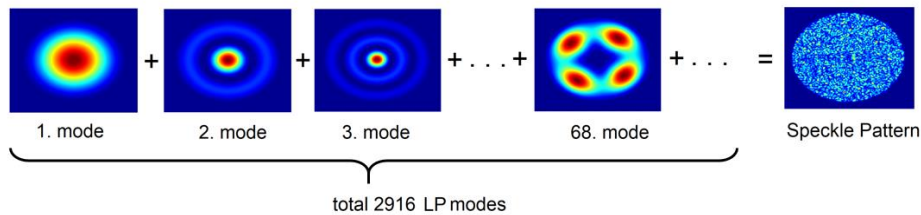

FIGURE 2. Formation of speckle pattern from fiber LP modes.

3. DESIGN AND IMPLEMENTATION

The simplest way to measure the response of an optical fiber to bending is to rotate it at diameter R. Optical fibers can be rotated in loop form up to a few cm in diameter without breaking or permanent deformation, as seen in Figure 3. As the loop radius decreases, a portion of the light escapes from the core to the cladding and is lost, resulting in a decrease in optical power at the fiber output. Although sensors based on the measurement of optical power change at the fiber output are quite practical compared to those using the interferometer principle, they are sensitive to noise and have low resolution due to power oscillations of the light source. Therefore we focused on the change of speckle pattern, not the change of optical power at the fiber output.
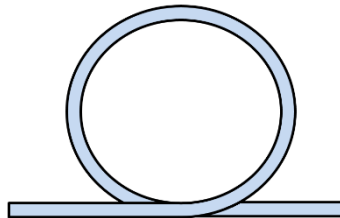

FIGURE 3. Design of fiber bending sensor for a full loop.

In this study, the optical fiber was rotated in the form of a ring with diameter R and the speckle pattern changes at the fiber end were obtained by using beam propagation method (BPM). This method is very useful for calculating the propagation of light in slowly changing waveguides. However, since the optical field

is calculated with the forward propagation algorithm, the backpropagation of light in waveguides such as ring fiber cannot be calculated. Therefore, we divided a fiber ring into equal arcs of 45 degrees as in Figure 4(a) and we obtained the speckle patterns by simulating in the forward propagation direction of the sensor, which has a form similar to an S-bend. In the simulation studies, we preferred to use a multimode fiber with core and cladding diameters of 105/125 um and NA = 0.22. The number of linear modes guided in this fiber is approximately 6000. To obtain the speckle pattern image, simulations must be performed in 3D propagation space. We have experienced that the simulation time for any value of the loop diameter took longer than a week on an ordinary computer. Therefore, by forming the fiber sensor with 6 equal arcs of 10 degrees as shown in Figure 4(b), we reduced the 3D propagation area and completed all simulation studies in a limited time.
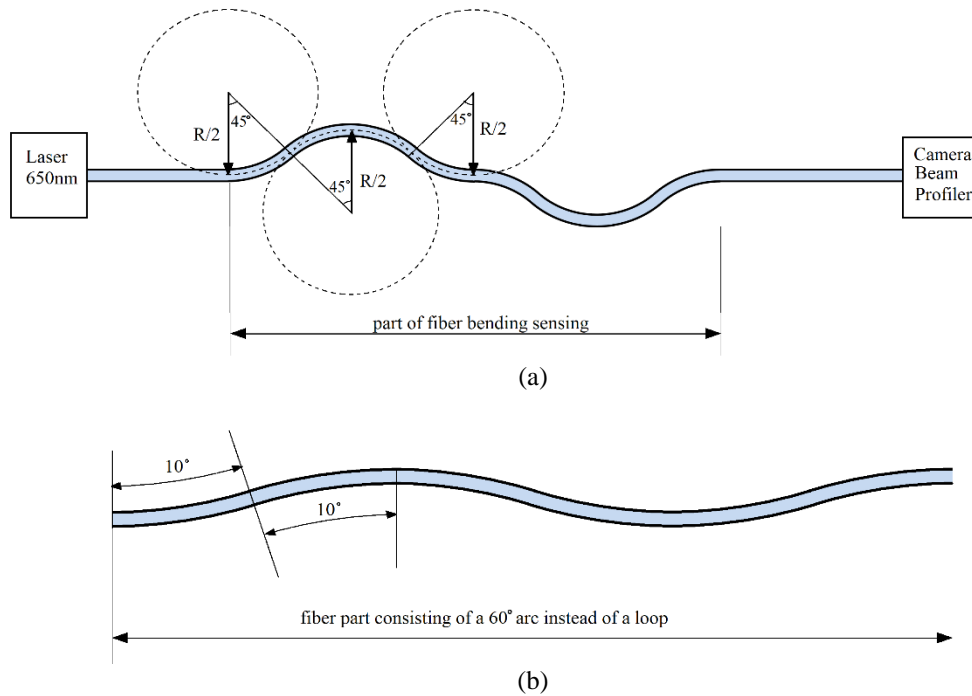

(a)

(b)

FIGURE 4. Design of S-bending like fiber sensor for simulation implementation in forward propagation a) sensor part whose bending consists of 8 arcs of 45 degrees b) sensor part whose bending consists of 6 arcs of 10 degrees.

In this study, we examined the effect of 60 degree S bending instead of full loop fiber. Of course, bending the fiber 60 degrees around a fixed radius may produce less changes in the speckle pattern than full bending. However, we have shown that bends as small as 60 degrees around different diameters can be detected by fiber speckle pattern imaging. We simulated bends created around different diameters in the range of 1-6 cm and recorded speckle pattern images at the fiber exit. Since approximately 4 cm of straight fiber part is added after bending, the total fiber length increases to 35.306 cm. The complex optical field propagating along the fiber was calculated in a 3D wafer using the BPM method.

Due to the S structure, the wafer resembles a rectangular prism. Wafer dimensions are adapted to the bending diameter. For a bending diameter of 6 cm, the X-Y cross-sectional area of the wafer is a rectangular plane with dimensions of 1100x126 micrometers as shown in Figure 5(a). Instead of the entire image on the wafer x-y plane, the process was continued with only the part containing the speckle pattern image by cropping and circular masking as shown in Figure 5(b). In addition, image enhancement operations such as background illumination correction and contrast enhancement were performed to achieve uniform illumination and image sharpness. Finally, we quantified how the similarity between consecutive images deteriorated as the bending radius changed by calculating the image correlation.

The cross correlation is a common method to quantify image similarity between two images [26]. As the similarity between images decreases, the correlation coefficient decreases from 1 to 0. Speckle pattern images contain many small-sized speckles. Calculating the average correlation coefficient by segmenting the image instead of the entire image gives better correlation for such images. As seen in Figure 5, the correlation between A and B images whose rows and columns are divided into M and N segments can be calculated as follows [27]:

$$C_{i,j} = \frac{\sum\left(A_{i,j} - \bar{A}\right)\left(B_{i,j} - \bar{B}\right)}{\sqrt{\sum\left(A_{i,j} - \bar{A}\right)^2\left(B_{i,j} - \bar{B}\right)^2}}$$

$$C = \frac{\sum C_{i,j}}{MxN}$$

In the next section, we showed that fiber bending can be detected by performing image correlation analysis by applying basic image processing functions.
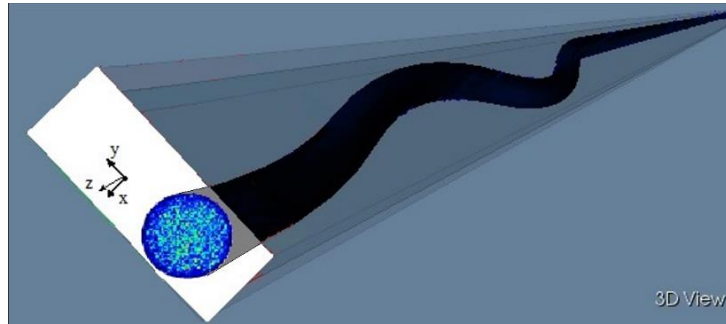
(a)
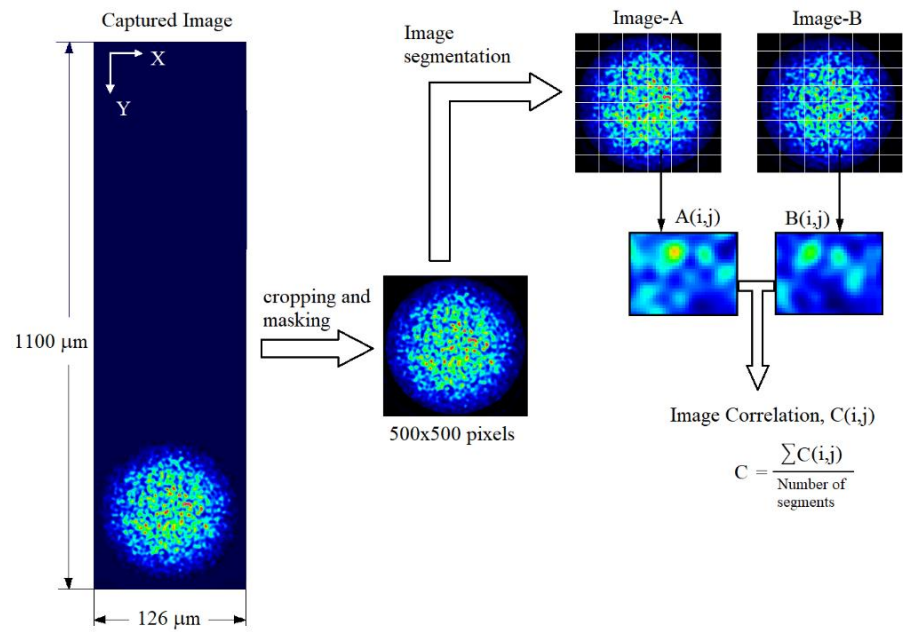
(b)

FIGURE 5. (a) 3D view of the wafer, (b) image processing steps.

4. RESULT AND DISCUSSION

We started the simulations with fiber bending with a diameter of 6 cm. The first image recorded at the fiber exit with a bending diameter of 6 cm was labeled as the reference image after applying the image processing steps. Then the bending diameter was increased by 2 μm in each new simulation and the last simulation was performed for a bending diameter of 6.0084 cm. Thus, 43 speckle pattern images were obtained. As the bending diameter changes, the sequential speckle pattern images obtained are very similar to each other. It is very difficult to notice the change when followed with the human eye. However, by performing correlation calculation on the segmented image as shown in Figure 5, the change from image to image is clearly visible. Figure 6 shows the variation of the correlation coefficient with a 2 μm diameter increase (ΔR) at each step around the 6 cm bending diameter of the fiber. In the correlation coefficient, the C(0) value is equal to 1 and this corresponds to the reference image (ΔR=0). After approximately the 40th image, the correlation drops below 0.1. This means that there is very little similarity between the two images.
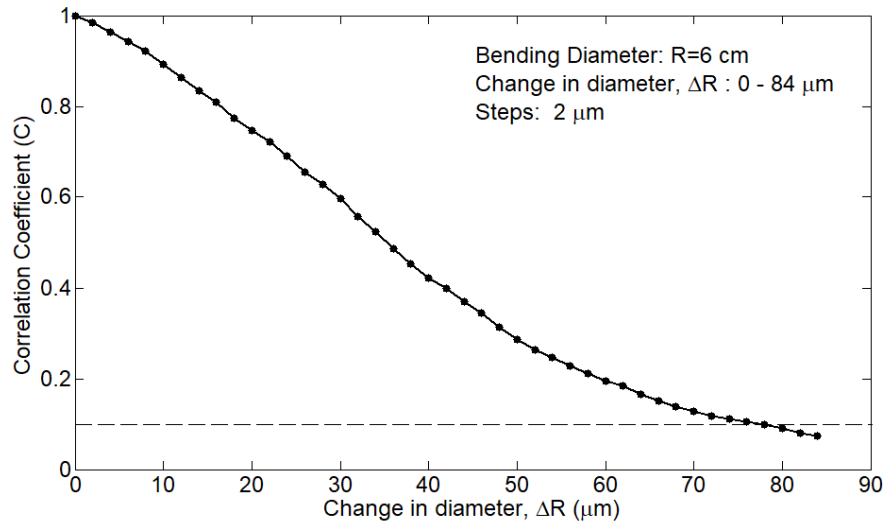

FIGURE 6. The variation of the correlation coefficient versus micrometer changes in bending diameter.

It is clearly seen in Figure 6 that diameter changes at 6 cm fiber bending gradually deteriorate the correlation. This can be explained by the fact that changes in bending

diameter affect the modes propagating along the fiber. However, it is quite remarkable that very small diameter changes such as 2 μm create measurable changes in the speckle pattern images. This result shows that very small changes in bending diameter can be measured by observing the fiber speckle pattern.

Although the field distributions of all guided modes in a straight fiber can be calculated theoretically, this situation is quite complicated in a bent fiber. Fiber curvature and bend-induced variations in the refractive index both tend to distort the mode field distributions [28]. Therefore, we can predict that as the bending diameter of the fiber decreases, there will be more severe distortions in the speckle pattern image. To verify this, we also tested our sensor for values of the bending diameter in the range of 1-6 cm, respectively. The distortion of correlation in the speckle pattern images was analyzed by changing the bending diameter in small steps of 2 μm, as in the experiment with bending diameter of 6 cm for this range. Figure 7 shows the variation of the correlation coefficient at different bending diameters.
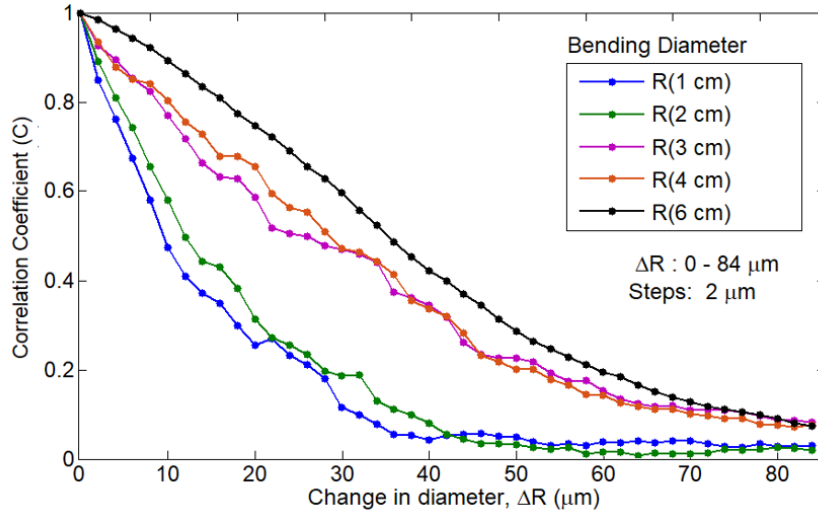

FIGURE 7. The variation of the correlation coefficient for different bending diameter.

It is clearly seen in Figure 7 that as the bending diameter decreases, micro-changes in diameter cause more severe correlation deterioration. The bending sensor with a diameter of 1 cm responds most sensitively to changes in diameter. We can simply define sensor sensitivity by $|\Delta C/\Delta R|$. Here, ΔC and ΔR are the change amounts in correlation and bending diameter, compared to the reference speckle pattern image ($C = 1$). If the diameter of the 6 cm bending sensor changes by 30 μm, the correlation coefficient drops to 0.5969 and thus its sensitivity is about 0.0013

μm^{-1}. On the other hand, for the bending sensor with a diameter of 1cm, the correlation coefficient drops to 0.1152, so its sensitivity is obtained as 0.0295 μm^{-1}. As a result, the small diameter bending sensor shows more severe correlation changes, which can be used to increase sensor sensitivity.

5. Conclusions

In this paper, a fiber bending sensor is proposed based on the correlation distortion in speckle pattern images. The bending sensor designed using a multimode fiber curved 60 degrees in a form similar to the S structure. The sensitivity of the sensor with different curvature diameters in the range of 1-6 cm was tested. The sensitivity was found to be 0.0013 μm^{-1} at 6 cm bending diameter and 0.0295 μm^{-1} at 1 cm bending diameter. It has been shown that the sensitivity increases as the bending diameter decreases. Our sensor can detect changes in the bending diameter at the μm level. We have demonstrated detection with only 60 degrees of S-structure bending. If the sensor structure is designed in the form of a loop, detection will be even more sensitive. On the other hand, the detection process is quite different from the methods applied in traditional fiber sensors. The detection principle of the proposed sensor is based on the processing of images with fiber speckle patterns, which offers a significant advantage for characterizing the sensor. Moreover, the sensor can be trained with deep learning algorithms and perform accurate measurements.

Author Contribution Statements The authors equally worked on this study. All authors contributed to this study at every stage.

Declaration of Competing Interests The authors declare that there is no conflict of interest regarding the publication of manuscript.

References

[1] Gao, H., Hu, H., Zhao, Y., Li, J., Lei, M., Zhang, Y., Highly-sensitive optical fiber temperature sensors based on PDMS/silica hybrid fiber structures, *Sens. Actuators A Phys.*, 284 (2018), 22-27, https://doi.org/10.1016/j.sna.2018.10.011.

[2] Su, H., Zhang, Y., Ma, K., Zhao, Y., Wang, J., High-temperature sensor based on suspended-core microstructured optical fiber, *Opt. Express,* 27 (2019), 20156, https://doi.org/10.1364/OE.27.020156.

[3]   Li, M., Gong, Y., Yin, J., Li, W., Shao, Y., Cong, A., Huang, G., Highly-sensitive and wide-range temperature sensor based on polymer-filled micro-cavity in fibre Bragg grating by temperature segmentation, *Optik*, 245 (2021), 167707.

[4]   Sun, X., Zhang, L., Zeng, L., Hu, Y., Duan, J., Micro-bending sensing based on single mode fiber spliced multimode fiber Bragg grating structure, *Opt. Commun.*, 505 (2022), 127513, https://doi.org/10.1016/j.optcom.2021.127513.

[5]   Perez-Herrera, R.A., Andre, R.M., Silva, S.F. et al., Simultaneous measurement of strain and temperature based on clover microstructured fiber loop mirror, *Measurement*, 65 (2015), 50-53, https://doi.org/10.1016/j.measurement.2014.12.052.

[6]   Bilsel, M., Navruz, I., Tapered optical fiber sensor for discrimination of strain and temperature, *Advances in Electrical and Electronic Eng.*, 18 (2020), 50-56.

[7]   Kissinger, T., Correia, R., Charrett, T. O. H., James, S. W., Tatam, R. P., Fiber segment interferometry for dynamic strain measurements, *J. Light. Technol.*, 34 (2016), 4620-4626, https://doi.org/10.1109/JLT.2016.2530940.

[8]   Sazio, P. J. A., Microstructured optical fibers as high-pressure microfluidic reactors, *Science*, 311 (2006), 1583-1586.

[9]   Dong, N., Wang, S., Jiang, L., Jiang, Y., Wang, P., Zhang, L., Pressure and temperature sensor based on graphene diaphragm and fiber Bragg gratings, *IEEE Photonics Technol. Lett.*, 30 (2018), 431-434, https://doi.org/10.1109/LPT.2017.2786292.

[10] Zhang, W., Ni, X., Wang, J., Ai, F., Luo et al., Microstructured optical fiber based distributed sensor for in vivo pressure detection, *J. Lightwave Technol.*, 37 (2019), 1865-1872.

[11] Kim, H. J., Shin, H. Y., Pyeon, C. H., Kim, S., Lee, B., Fiber-optic humidity sensor system for the monitoring and detection of coolant leakage in nuclear power plants, *Nucl. Eng. Technol.*, 52 (2020), 1689-1696.

[12] Bian, C., Wang, J., Bai, X., Hu, M., Gang, T., Optical fiber based on humidity sensor with improved sensitivity for monitoring applications, *Opt. Laser Technol.*, 130 (2020), 106342.

[13] Zhang, J., Shen, X., Qian, M., Xiang, Z., Hu, X., An optical fiber sensor based on polyimide coated fiber Bragg grating for measurement of relative humidity, *Opt. Fiber Technol.*, 61 (2021), 102406, https://doi.org/10.1016/j.yofte.2020.102406.

[14] Huang, X. Lai, M., Zhao, Z., Yang, Y. et al., Fiber optic evanescent wave humidity sensor based on SiO_2/TiO_2 bilayer films, *Appl. Opt.*, 60 (2021), 2158-2165.

[15] Wang, T., Yasukochi, W., Korposh, S., James, S. W., Tatam, R. P., Lee, S.-W., A long period grating optical fiber sensor with nano-assembled porphyrin layers for detecting ammonia gas, *Sens. Actuators B*, 228 (2016), 573-580.

[16] Yu, C.-B., Wu, Y., Li, C., Wu, F., Zhou, J.-H., Gong, Y., Rao, Y.-J., Chen, Y.-F., Highly sensitive and selective fiber-optic Fabry-Perot volatile organic compounds sensor based on a PMMA film, *Opt. Mater. Express*, 7 (6) (2017), 2111-2116.

[17] Sultangazin, A., Kusmangaliyev, J., Aitkulov, A., Akilbekova, D., Olivero, M., Tosi, D., Design of a smartphone plastic optical fiber chemical sensor for hydrogen sulfide detection, *IEEE Sens. J.*, 17 (21) (2017), 6935-6940.

[18] Hosok, A., Nishiyama M., Kumekawa N., Watanabe, K. Et al., Hetero-core structured fiber optic chemical sensor based on surface plasmon resonance using Au/lipid films, *Opt. Commun*., 524 (2022), 128751, https://doi.org/10.1016/j.optcom.2022.128751.

[19] Wu, Y., Pei, L., Jin, W., Youchao, J., Yang, Y., et al., Highly sensitive curvature sensor based on asymmetrical twin core fiber and multimode fiber, *Opt. Laser Technol.*, 92 (2017), 74-79, https://doi.org/10.1016/j.optlastec.2017.01.007.

[20] Gong, Y., Zhao, T., Rao, Y-J., Wu, Y., All-fiber curvature sensor based on multimode interference, *IEEE Photonics Technol*. *Lett*., 23 (2011), 679-681.

[21] Li, Y-P., Zhang, W-G., Wang, S., Chen, J. et al., Bending vector sensor based on a pair of opposite tilted long-period fiber gratings, *IEEE Photonics Technol*. *Lett*., 29 (2017), 224-227, https://doi.org/10.1109/LPT.2016.2636446.

[22] Chen, Y., Yu, Z., Chen, H., Tao, C., et al., Experimental study on temperature-insensitive curvature sensor based on reflective all-fiber structure, *Infrared Phys. Techn.*, 137 (2024), 105146, https://doi.org/10.1016/j.infrared.2024.105146.

[23] Anderson, D. Z., Bolshtyansky, M. A., and Zel'dovich, B. Y., Stabilization of the speckle pattern of a multimode fiber undergoing bending, *Opt. Lett.*, 21 (11) (1996), 785-787.

[24] Asawa, C. K., Taylor, H. F., Propagation of light trapped within a set of lowest-order modes of graded-index multimode fiber undergoing bending, *Appl. Opt.*, 39 (2000)**,** 2029-2037.

[25] Keiser, G., Optical Fiber Communication, Mc Graw Hills, Third Edition, Singapore, 2000.

[26] Schreier, H., Orteu, J-J., Sutton, M. A., Image correlation for shape, motion and deformation measurements, Springer, 2009.

[27] Ari, F., Serbetci, H., Navruz, I., Tapered fiber optic refractive index sensor using speckle pattern imaging, *Opt. Fiber Technol*., 79 (2023), 103366.

[28] Schermer, R. T., Mode scalability in bent optical fibers, *Optics Express*, 15 (24) (2007), 15674-15701, https://doi.org/10.1364/OE.15.015674.